Copy No._____

Defence Research and Development Canada
Recherche et développement pour la défense Canada

DEFENCE R&D DÉFENSE

# A Review of Submarine Out-of-Plane Normal Force and Pitching Moment

*M. Mackay*

**Defence R&D Canada – Atlantic**

Technical Memorandum
DRDC Atlantic TM 2004-135
August 2004

Canada

This page intentionally left blank.

Copy No. _____

# A Review of Submarine Out-of-Plane Normal Force and Pitching Moment

M. Mackay

**Defence R&D Canada – Atlantic**

Technical Memorandum
DRDC Atlantic TM 2004–135
August 2004

Author

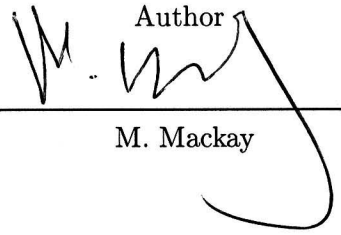

M. Mackay

Approved by

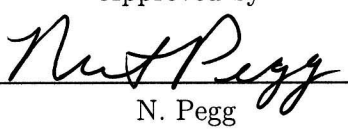

N. Pegg
Head, Warship Performance

Approved for release by

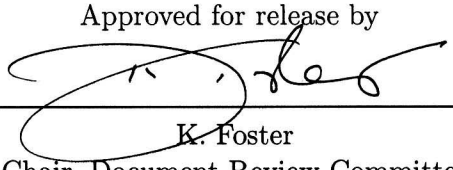

K. Foster
Chair, Document Review Committee

## Abstract

This memorandum summarizes the comparison of a simple out-of-plane load estimation method with model test data for a number of submarine designs. Out-of-plane loads can be reasonably estimated from sail lift by assuming that the bound afterbody circulation falls roughly linearly to zero at the tail. Tail appendages have very little effect on these loads.

## Résumé

Cette étude résume la comparaison d'une méthode simple d'estimation des charges hors-plan en fonction des données d'essais sur modèle de divers sous-marins. Une estimation raisonnable des charges hors-plan peut être obtenue à partir de la poussée au niveau du kiosque en supposant que l'écoulement vers l'arrière diminue de façon constante à l'arrière du kiosque. Les appendices à ce niveau ont très peu d'effet sur ces charges.

This page intentionally left blank.

## Executive Summary

### Introduction

The normal force and pitching moment experienced by a submarine in a turn, or at an angle of drift, are called 'out-of-plane' because they are loads induced in the vertical plane by a manoeuver in the horizontal plane. They arise from the interaction of flow circulation generated by the sail with crossflow on the hull aft of the sail, i.e., the Magnus Effect.

### Significance

Smaller than the corresponding in-plane loads, sideforce and yawing moment, the out-of-plane loads are nevertheless significant for good manoeuverability and safety. Left uncorrected, they would result in a bow-up attitude and decrease in depth, but are generally not a significant problem for closed-loop control. However, while this response may assist recovery from a plane jam-to-dive, it could hinder covert recovery from a jam-to-rise. It is necessary to model out-of-plane loads in a numerical simulation.

### Principal Results

Experiments with a number of submarine configurations validate the previously proposed linear circulation distribution model, or a simple modification of it, for estimating the out-of-plane normal force and pitching moment arising from both drift and yaw rate. The effect of the tail does not appear to be greatly significant. Pitching moment may be underpredicted for submarines with a relatively small sail.

### Further Work

A numerical circulation distribution model will be implemented in the `DSSP21` manoeuvering simulation code for estimating out-of-plane loads. In the longer term, the effect of full scale Reynolds numbers should be investigated so that proper scaling can be applied to results from experimental and numerical models.

M. Mackay, 2004. A Review of Submarine Out-of-Plane Normal Force and Pitching Moment. DRDC Atlantic TM 2004–135. Defence R&D Canada – Atlantic.

## Sommaire


### Introduction

La force normale et le moment de tangage subis par un sous-marin en virage ou à un angle de dérive sont ≪hors-plan≫ car il s'agit de charges induites sur le plan vertical par une manœuvre sur le plan horizontal. Elles sont créées par l'interaction entre l'écoulement hydrodynamique générée par le kiosque et l'écoulement transversal sur la coque à l'arrière du kiosque, c'est-à-dire l'effet Magnus.

### Importance

Plus petites que les charges dans le plan correspondantes, la force latérale et le moment de lacet, les charges hors-plan sont néanmoins importantes pour obtenir une bonne manœuvrabilité et assurer la sécurité. Si elles n'étaient pas corrigées, ces forces provoqueraient la levée du nez et une diminution de la profondeur, mais en général elles ne constituent pas un problème pour un contrôle en boucle fermée. Toutefois, bien que cette réaction puisse contribuer au rétablissement à la suite du coincement des barres de plongée vers le bas, elle pourrait gêner le rétablissement à la suite du coincement des barres de plongée vers le haut. Une modélisation des charges hors-plan dans une simulation numérique est nécessaire.

### Résultats principaux

Des expériences avec un certain nombre de configurations de sous-marin rendent valide le modèle de répartition de l'écoulement linéaire qui a déjà été proposé, ou une simple modification de ce modèle, pour l'estimation de la force normale hors-plan et du moment de tangage créés par la dérive et le lacet. La présence des barres et des gouvernails ne semble pas avoir une grande importance. Le moment de tangage peut rester imprévisible pour les sous-marins munis d'un kiosque relativement petit.

### Autres travaux

Un modèle numérique de répartition sera mis en œuvre dans le code de simulation de manœuvre `DSSP21` afin d'évaluer les charges hors-plan. À plus long terme, l'effet en vraie grandeur du nombre de Reynolds doit être édudié afin d'appliquer l'échelle appropriée aux résultats des modèles expérimentaux et numériques.



M. Mackay, 2004. A Review of Submarine Out-of-Plane Normal Force and Pitching Moment. DRDC Atlantic TM 2004–135. R & D pour la défence Canada – Atlantique.

# Table of Contents

## List of Figures



## Acknowledgments


Thanks are due to Peter Butterworth and David Atkins, both of QinetiQ, for their discussion and interpretation of the DERA rotating arm and static drift test results.

# 1 Introduction

The basis for submarine out-of-plane force and moment calculation is under review for incorporation into the DSSP21 manoeuvering simulation code. This document summarizes validation of a proposed method with model test data.

These loads are primarily generated by the interaction of circulation on the hull with crossflow, a phenomenon familiar as the Magnus Effect. The hull circulation is caused by upstream geometric asymmetry: for the present discussion, by the sail on the submarine. However, the principles outlined here apply to any appendage large enough to generate circulation in crossflow, e.g., the deep keel found on some UUVs. While there may be other mechanisms contributing to out-of-plane loads, propulsor interactions for example, the present discussion is confined to the definition above.

The normal force and pitching moment experienced by a submarine in a turn, or at an angle of drift, are called 'out-of-plane' because they are loads induced in the vertical plane by a manoeuver in the horizontal plane. Smaller than the corresponding in-plane loads, sideforce and yawing moment, they nevertheless have an impact on manoeuverability and safety. Left uncorrected, they would result in a bow-up attitude and decrease in depth, but are generally not a problem for maintaining closed-loop control although several degrees of sternplane deflection may be required to offset their effect. This deflection may limit the remaining control authority, and the associated drag affects manoeuvering characteristics such as speed loss in a turn. In an emergency, while the out-of-plane response can assist recovery from a plane jam-to-dive, it could hinder covert recovery from a jam-to-rise.

In establishing the manoeuvering characteristics of a submarine, it is therefore necessary to estimate the out-of-plane loads with sufficient accuracy to derive the corrective plane deflections and emergency recovery implications. Since for some small vehicle configurations the out-of-plane loads could be relatively larger, it is important to be able to assess their impact on the controllability of a UUV.

Background work on the problem has been previously published by the author in references [1] to [3]. The key was shown to be the distribution of circulation on the hull aft of the sail: simply using the circulation strength derived from potential flow theory greatly overpredicted the out-of-plane loads. An initial survey of static drift experiments with members of the Standard Model series [1] suggested that a reduction of hull-bound circulation in proportion to drift angle gave more consistent agreement than piecewise distributions such as proposed by Feldman [4]. In subsequent investigations of the apparent loss of circulation, good prediction of the out-of-plane loads was obtained using the CANAERO panel code to model crossflow separation on the hull. The separation resulted in circulation falling more-or-less linearly to zero from the sail to the tail [2], and this distribution was corroborated by integrating static pressures measured on the afterbody of a wind tunnel model [2,5]. A further investigation using panel code modeling showed that the presence of a deck casing had very little effect on the out-of-plane loads [3].

Accumulation of new data since that work has allowed a review of the problem and a re-examination of the applicability of a simple model, such as the linear circulation distribution, for numerical simulations. This memorandum presents validation of the linear model, and variants, with a number of submarine geometries, and gives limited validation for crossflow derived from both static drift and rotation in yaw. Acronyms found in the text are listed under Nomenclature.

## 2 Origin of the Out-of-Plane Loads

This section summarizes the descriptions given in references [1] and [3] and illustrated in figure 1. In the simple case of constant drift $\beta$, circulation $\Gamma$ convected from the sail is shed at the tip and bound to the body; the shed vortex gives rise to only secondary effects and is neglected for this analysis. The bound afterbody vortex gives rise to a downward normal force per unit length $\widehat{Z}$ according to the Kutta-Joukowski Theorem:

$$\widehat{Z} = -\rho v \Gamma \tag{1}$$

where $\rho$ is density and $v$ the crossflow velocity. The out-of-plane normal force $Z$ and pitching moment $M$ are the integrals of $\widehat{Z}$ and of the first moment of $\widehat{Z}$, respectively, taken over the afterbody.

Setting $\Gamma$ uniformly equal to the sail circulation $\Gamma_{sail}$ greatly overpredicts $Z$ and $M$. However, since the bound circulation is derived from the sail circulation, it can be expressed as $f(x)\Gamma_{sail}$, where $f(x)$ is a distribution function to be determined. In addition, for an arbitrary horizontal plane manoeuver the local crossflow velocity varies along the axial coordinate, so equation (1) becomes

$$\widehat{Z}(x) = -\rho v(x) f(x) \Gamma_{sail} \tag{2}$$

where $\widehat{Z}(x)$ is the load distribution, or local unit normal load, on the afterbody.

For the present purpose, it is more convenient to express the load distribution in terms of lift (in boat coordinates, the sideforce) on the sail, $Y_{sail} = \rho U \Gamma_{sail} b_e$, where $U$ is total velocity and $b_e$ is the effective span of the sail. With this substitution, and the quantities nondimensionalized in the usual manner [4], equation (2) becomes:

$$\widehat{Z}'(x') = \frac{-v'(x') f(x') Y'_{sail}}{b'_e} \tag{3}$$

and the nondimensional out-of-plane loads are:

$$Z' = \int_{x'_{AP}}^{x'_{TE}} \widehat{Z}'(x') dx' \qquad \text{and} \qquad M' = -\int_{x'_{AP}}^{x'_{TE}} x' \widehat{Z}'(x') dx' \tag{4}$$

The limits of integration, shown here as the sail trailing edge, $x'_{TE}$, and the aft perpendicular, $x'_{AP}$, define the extent of the afterbody bound vortex for the purpose of estimating loads, and should be consistent with the parameters of $f(x')$.

# 3 The Standard Model in Drift

The geometry of the Standard Model and its static hydrodynamic characteristics are reviewed in reference [6], which also gives procedural details of the individual test series (NAE, MARIN, STR, DERA, and MDTF) referred to here. Test configuration HS is the hull and sail alone; configuration HST is the hull, sail, and tail. Since data for this and for the other submarines discussed below are for the most part proprietary, ordinate scales, apart from the zero, have been omitted from the figures.

## 3.1 Out-of-Plane Load Characteristics

Figure 2 depicting HS and HST out-of-plane force and moment data has been taken from reference [6] and replotted with the same vertical scales for each configuration. Between 15 and 20 degrees drift the data exhibit a reflex characteristic, resulting in reduced loads at the larger angles. Unfortunately, this observation is based largely on the STR results — the other tests have fewer data past this region — for which there is a question regarding the reliability of tunnel corrections to $Z'$ and $M'$ at high angles of drift [7]. Other results suggest that a fall-off in loads is either less or delayed to higher drift angles, and is largely confined to the pitching moment, which is more susceptible to the effect of flow separation at the tail. In none of the experiments does the fall-off correlate well with sail stall. Since all the data incorporate, to a greater or lesser degree, uncorrected effects such as support interference, or surface and tank boundary proximity at large drift angles [6], it remains moot whether the fall-off in these loads would occur in the same range of drift angles on a free model — resulting perhaps from tail flow separation — or whether it is an artifact of the experiments. Similarly contradictory results have been found for other submarine models. Consequently, validating the out-of-plane load predictions described below has concentrated on experimental data for drift angles up to about 15 degrees.

The other obvious feature of figure 2 is scatter in the data, illustrating that these loads are relatively difficult to measure accurately in the presence of the larger (often, much larger) in-plane loads. In addition to the inevitable random errors in measurement, there are systematic ones, generally in the form of an offset in the load or in the drift angle. $Z'$ should be essentially zero, and $M'$ slightly positive (because of sail drag), for an unpowered model at zero drift, so long as the coordinate origin is, as usual, on the hull axis. A significant deviation in either could be caused by model bending or by misalignment. For similar reasons, the loads at small drift angles may not be symmetric about the zero; indeed, $Z'$ and $M'$ can be independently asymmetric. In the presentations of $Z'$ and $M'$ that follow, both load and drift angle offsets have been removed from the data to facilitate comparison with numerical predictions. Residual data asymmetry at large drift angles is generally the result of facility boundary interference.

## 3.2 Effect of the Tail

Since there are partial load distributions (from static pressure measurements) for both HS and HST configurations from the DERA experiments, and a more complete distribution for the HS configuration from the NAE experiments, these results are of particular interest. They have been extracted from the previous figure and replotted on figure 3 with the data offsets removed. It is not possible to confidently quantify random and residual systematic errors for data presented in this fashion. Estimates in reference [6] of systematic error lower bounds were up to 30 percent for $Z'$ and 12 percent for $M'$. However, after removing offsets, scatter and other visible discrepancies in the figures are probably a better guide.

The tail has little effect on downforce, but appears to increase pitching moment at drift angles above about 10 degrees. The Standard Model has somewhat larger than typical tailplanes, which may influence tail flow separation. There is, however, little apparent difference (within experimental scatter) between the DERA and NAE HS data, despite the former having a clean, untruncated, tail, whereas the latter's tail was truncated for a sting support [6].

## 3.3 Afterbody Load Distribution

Reference [1] discussed piecewise uniform load distributions and their effect on the out-of-plane loads for a number of variants in the Standard Model systematic series. It was observed that while these distributions could be constructed to agree with the experimental data, an underlying physical basis was lacking. Incorporating afterbody separation into the model with a new version of the `CANAERO` panel code showed the load distribution diminishing essentially linearly from the sail to the tail, which was confirmed by static afterbody pressure measurements in the NAE experiments [2,3] at four stations: 5, 6, 7, and 8, where station 0 is the FP and station 10 is the AP.

Afterbody pressures at the same four stations were also measured in the 1996 DERA static experiments [8]; provision for this was a requirement in earlier rotating arm tests with the same model, described in section 5. Unfortunately, only half the pressure taps at stations 5 and 6 were monitored because the required number of scanivalve units could not be accommodated in the static test arrangement, so $\widehat{Z}'$ has been derived for stations 7 and 8 only. Comparison with `CANAERO` and the NAE results is made in figure 4 for four comparable drift angles; the experimental angles did not all exactly coincide. A linear fit is indicated for the DERA results, and a locally-weighted regression fit for the NAE results. The departure from linearity of the latter may be due to sensitivity to alignment on the tail cone of the disc probes that were used [5].

Linear fits to the DERA load distributions for the HS and HST configurations are compared in figure 5. Although approaching the limit of experimental error, the trend indicates that aft loading is somewhat higher in this region when the tail is present (HST), notably at large drift angles. The previous observation that the tail had little

effect on the downforce but increased pitching moment at drift higher than 10 degrees therefore implies that there was little significant effect of the tail at stations 5 and 6. Plotting $\widehat{Z}'$ against drift for stations 7 and 8, figure 6, indicates that the effect of the tail on the load distribution may be at the threshold of experimental uncertainty at station 7, and a little above it at station 8.

# 4 A General Aft Loading Prediction Method

The foregoing observations are consistent with the linear loading model proposed in reference [3], or an approximation of it. A more general form of the model is:

$$\begin{aligned} f(x') &= 1 && x' \geq x'_1 \\ &= \left[\frac{x' - x'_2}{x'_1 - x'_2}\right]^{m(\beta_c)} && x'_1 > x' > x'_2 \\ &= 0 && x'_2 \geq x' \end{aligned} \tag{5}$$

In which $x'_1$ and $x'_2$ define the ends of the ramp, and $m(\beta_c)$, where $\beta_c$ is some critical drift angle, modifies the form of the distribution. For pure drift, $\beta_c = \beta$. If $m = 1$ the load distribution is linear. A simple way to represent the influence of drift angle is to use $m = 1 + k\beta_c$, where $k$ is a constant.

In general, $x'_1$ is in the vicinity of the sail trailing edge, and $x'_2$ is in the vicinity of the AP. In comparisons made to date with experimental data there has been little to justify altering these parameters, so in every case illustrated below $x'_1 = x'_{TE}$ and $x'_2 = x'_{AP}$.

For the following comparisons sail lift was predicted by the `DSSP20` code [9,10] and $b_e$ is the effective span `BEFF` calculated by the program. The predictions have no zero drift offsets.

## 4.1 Application to the Standard Model

Figure 7 repeats the comparisons previously shown in figure 3 with the addition of MARIN HS data, and curves for a linear load distribution and for $m = 1 + 3\beta$ (with $\beta$ in radians). The MARIN data are included because they constitute the test case Submarine A in reference [1]. Up to about 10 degrees, the linear distribution curve is a reasonable approximation to both $Z'$ and $M'$ while the nonlinear one is a lower bound to the data. Since the linear distribution better fits the HST moment data, it is the preferred load model.

## 4.2 Other Validation for Pure Drift

Comparison of predicted and experimental loads for a number of other submarine models are shown in figure 8. Predictions were done with a linear load distribution and, where the fit might be improved, with a nonlinear distribution as indicated on the figures.

The first four pairs of graphs on this figure are for test cases Submarines B to E in reference [1]. They are HS configuration variants from the Standard Model systematic series, comprising the parent hull with:

- Submarine B: parent sail moved forward,
- Submarine C: parent sail moved aft,
- Submarine D: high aspect ratio sail, and
- Submarine E: low aspect ratio sail.

The tests were all performed at MARIN. There are some tank bottom and surface proximity effects in these data at high drift angles. At drift angles below 10 degrees the linear model generally gives reasonable predictions; however, the Submarine C normal force is an exception, and the Submarine D pitching moment data show clear discrepancies at 5 degrees.

The last five pairs of graphs in figure 8 are representative configurations with different geometry and, in most cases, self-propulsion during the model test. The following list is a qualitative summary of their parameters with respect to a typical modern diesel-electric submarine, denoted 'Avg.'. One model has X–rudders ('$\times$'), the rest have a cruciform tail ('+').

| Model | Hull Slenderness | Sail Dimensions | Tail Arrangement | Propulsion in Test |
|---|---|---|---|---|
| UC | $>$ Avg. | $>$ Avg. | + | Yes |
| UD | $>$ Avg. | $<$ Avg. | + | No |
| UH | $<$ Avg. | $<$ Avg. | + | Yes |
| UJ | $>$ Avg. | $<$ Avg. | + | Yes |
| UT | $<$ Avg. | Avg. | $\times$ | Yes |

There is no apparent correlation of these parameters with the goodness-of-fit of the predictions other than that a small sail does not appear to favour matching both $Z'$ and $M'$ with the same model (the linear model is satisfactory for $Z'$ while $m < 1$ is required to match $M'$). A similar observation can be made for Submarine D, which had half the sail chord of the others in that series.

While questions remain regarding the effect of sail geometry, the results in figure 8 allay to some extent the pessimism expressed in reference [3] regarding the likelihood of formulating a simple, general, model to predict the out-of-plane loads.

Apart from the Standard Model, the only other source of afterbody load distributions that the author is aware of is Ward and Wilson [11]. They tested a bare hull (H) and a

HS configuration with the sail fairly far forward, measuring pressures on the afterbody and in the flow field. Total model loads were unobtainable with their test arrangement.

Distributions derived from the integrated pressures are shown in figure 9. The bare hull normal loads, which should be zero, are largely attributable to non-axial flow in the test facility [11]. A first order correction to the out-of-plane load distribution is therefore obtained by subtracting the bare hull results from those of the HS configuration. The results are compared with linear and $m = 1 + 3\beta$ predictions in figure 10. The agreement in this figure is satisfactory, especially since the test Reynolds number was quite low: about 2.4 million based on hull length.

## 5 Rotating Arm Validation for the Standard Model

The generalized prediction model as represented by equations (3), (4), and (5) is equally applicable to a submarine in a steady turn. Although the contribution of curvature (the nondimensional yaw rate $r'$) in $v'(x') = -\tan\beta + x'r'$ for a purely horizontal plane manoeuver is generally less than that of drift, confirmation of its effects was sought. Unfortunately, there are few model data that permit the effect of rotation on the out-of-plane loads to be assessed in detail.

The Standard Model was tested on the DERA rotating arm in 1991 in the parent HS configuration, and again in 1994 in the HST configuration. Total loads and static pressures at stations 5, 6, 7, and 8 on the afterbody were measured. A description and analysis of the 1991 tests have been given by Butterworth [12]; the 1994 tests are hitherto unpublished. Results in this section are reported at angle of yaw rather than drift for consistency in cross-comparisons. Yaw was the angle set on the model support turntable; it differed from drift at the coordinate origin by up to three degrees [12].

HS and HST experimental load distributions from integrated pressures are shown for four curvatures and five yaw angles in figure 11. All parts of the figure are plotted to the same vertical scale. Curvature has virtually no effect on the loading within experimental uncertainty. The effect of the tail is to increase loading at the highest yaw angles and to decrease it at the smaller angles. At large yaw angles the loading drops to zero at or (at higher curvature) before station 8; there is no indication of load recovery further aft.

The out-of-plane loads are plotted, together with predictions using linear and nonlinear ($m = 1 - 2\beta$) circulation models in figure 12. Rotation precludes removing data yaw offsets as in previous figures, and uncertainty in matching the numerical models is therefore higher than for pure drift. The data rise faster than the predictions up to about 10 degrees yaw for the HS configuration, and a little higher for the HST configuration, after which they tend to fall off towards zero (HS) or to plateau (HST). There is reason to believe that this fall off is in part, if not entirely, an artifact of support interference. In the correction runs of these experiments the wake of the vertical support strut would have intersected the tail of the model at 15 degrees yaw,

and its effects would have been felt at smaller angles. Although the effects were, to first order, canceled out in the correction procedure, a residual impact on the relatively small out-of-plane loads cannot be discounted — and would be consistent with the observation that the large yaw angle load distributions fall to zero forward of the tail.

In figure 13 the load distributions for 5, 10, and 15 degrees are compared with predictions based on a linear circulation distribution. Numerical predictions are reasonable at 15 degrees and somewhat less than the experimental values at smaller yaw angles.

## 6 Concluding Remarks

The model experiment validations presented in this memorandum give sufficient confidence to use a simple, or modified, linear circulation distribution model for estimating submarine out-of-plane normal force and pitching moment in the `DSSP21` simulation code. Although corroboration of secondary effects such as those of the tail and yaw rate is sparse, the effects did not appear to be greatly significant in the experimental data examined here. A relatively small sail in four of the nine test cases may be associated with underprediction of the pitching moment. Without considerably more data, the connection is speculative: possibilities include support interference or Reynolds number effects. Further work to be done includes investigation into the effect of full scale Reynolds numbers so that proper scaling can be applied to predictions from experimental and numerical models.

## References


1. Mackay, M. (1988). The Prediction of Submarine Out-of-Plane Force and Moment using a Panel Method. In *Warship '88 International Symposium on Conventional Naval Submarines*. London: The Royal Institution of Naval Architects.

2. Conway, J.T. and Mackay, M. (1990). Prediction of the Effects of Body Separation Vortices on Submarine Configurations using the CANAERO Panel Method. AIAA 28th Aerospace Sciences Meeting, Reno. (AIAA paper 90–0302). American Institute of Aeronautics and Astronautics.

3. Mackay, M. and Conway, J.T. (1991). Modelling the Crossflow Body Separation on a Submarine using a Panel Method. In *Warship '91 International Symposium on Naval Submarines 3*. London: The Royal Institution of Naval Architects.

4. Feldman, J. (1979). DTNSRDC Revised Standard Submarine Equations of Motion. (DTNSRDC SPD–0393–09). David Taylor Naval Ship Research and Development Center.

5. Mackay, M. (1990). Static Pressure Measurement with Surface-Mounted Disc Probes. *Experiments in Fluids*, Vol. 9, No. 1/2.

6. Mackay, M. (2003). The Standard Submarine Model: A Survey of Static Hydrodynamic Experiments and Semiempirical Predictions. (DRDC Atlantic TR 2003–079). Defence R&D Canada – Atlantic.

7. Nguyen, V.D., Drolet, Y., and Watt, G.D. (1995). Interference of Various Support Strut Configurations in Wind Tunnel Tests on a Model Submarine. (AIAA paper 95–0443). AIAA 33rd Aerospace Sciences Meeting, Reno, Nevada. American Institute of Aeronautics and Astronautics.

8. Atkins, D.J. (1999). The Application of Computational Fluid Dynamics to the Hydrodynamic Design of Submarines. In *Warship '99 International Symposium on Naval Submarines 6*. London: The Royal Institution of Naval Architects.

9. Mackay, M. (1999). DSSP20 (Beta Edition) User Guide to the Preprocessing Modules. (DREA TM 1999–108). Defence R&D Canada – Atlantic.

10. Mackay, M. (1999). DSSP20 (Beta Edition) User Guide to the Simulation Modules. (DREA TM 1999–109). Defence R&D Canada – Atlantic.

11. Ward, B. and Wilson, P.A. (1992). Forces on a Body of Revolution in a Vortex Flow Field. In *Transactions of the Royal Institution of Naval Architects*, Vol. 134. London: The Royal Institution of Naval Architects.

12. Butterworth, P.J. (1993). The Measurement of Forces, Moments, and Static Pressures on a Model Submarine. (DRA/AWMH/TR93023). Defence Research Agency. Limited Distribution.

This page intentionally left blank.

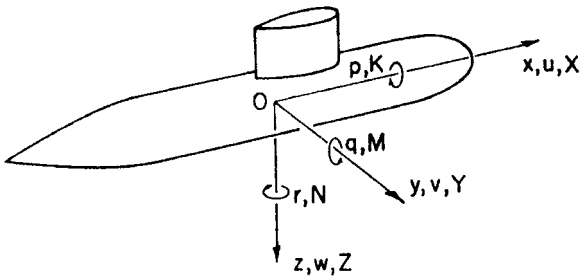


(a) Standard submarine coordinate convention; $\beta = \tan^{-1}(-v/u)$.

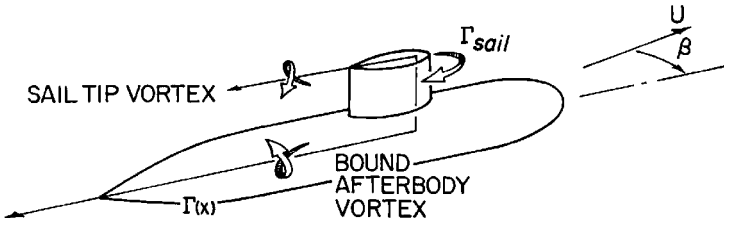


(b) Basic circulation model.

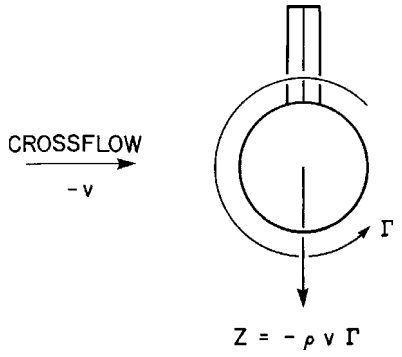


(c) Force on an isolated afterbody vortex.

**Figure 1.** Origin of the out-of-plane loads; from reference [1].

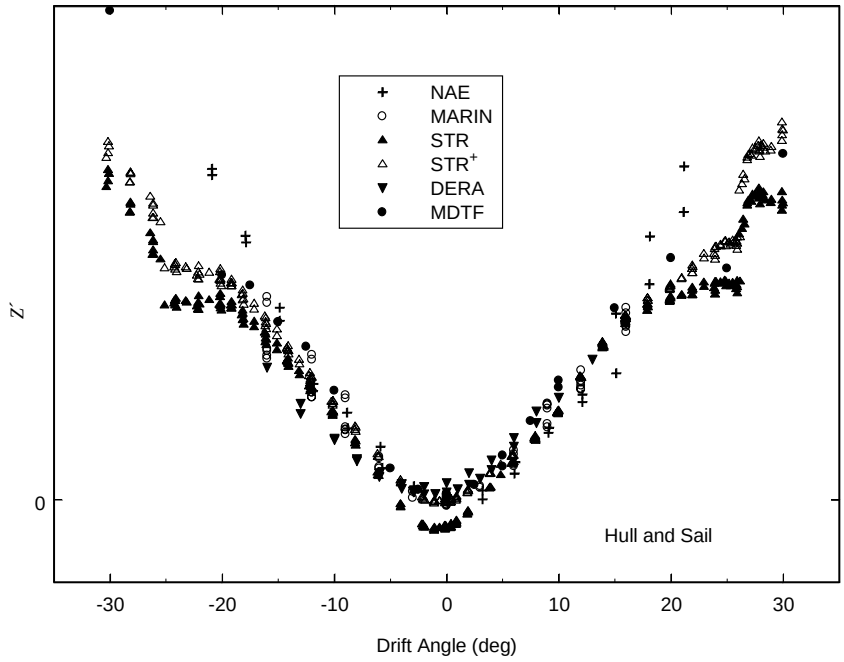


(a)

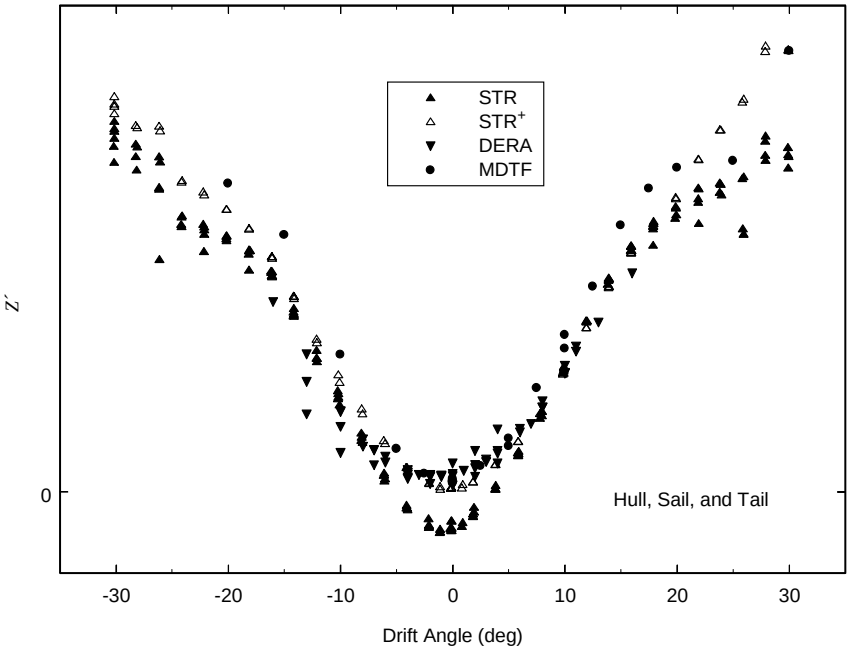


(b)

**Figure 2.** Standard Model out-of-plane normal force: (a) HS and (b) HST configurations; from figures 30 and 62 of reference [6]. The notation $STR^{+}$ indicates STR runs to which additional corrections were applied. (continued)

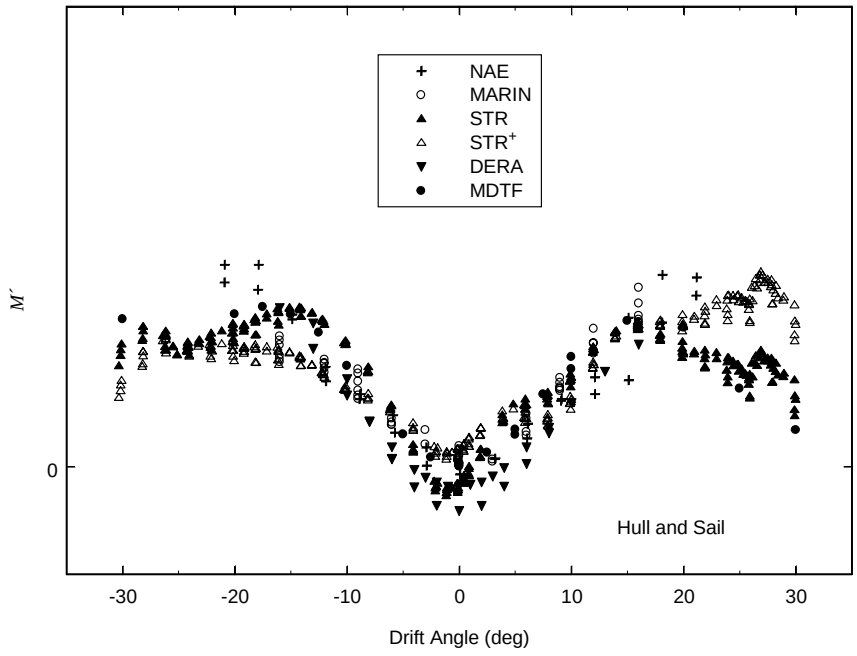


(c)

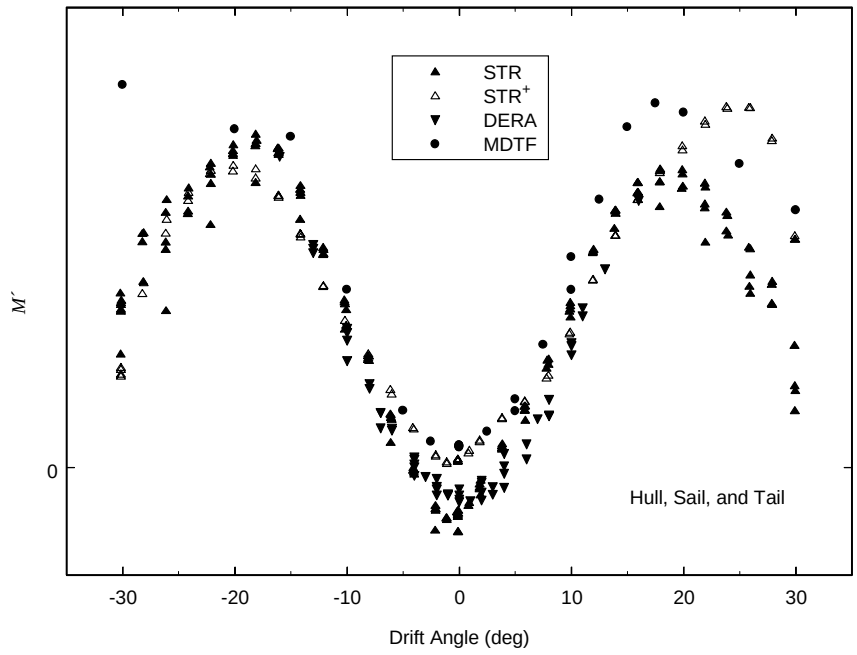


(d)

**Figure 2. (cont.)** Standard Model out-of-plane pitching moment: (c) HS and (d) HST configurations; from figures 32 and 64 of reference [6]. The notation $STR^{+}$ indicates STR runs to which additional corrections were applied.

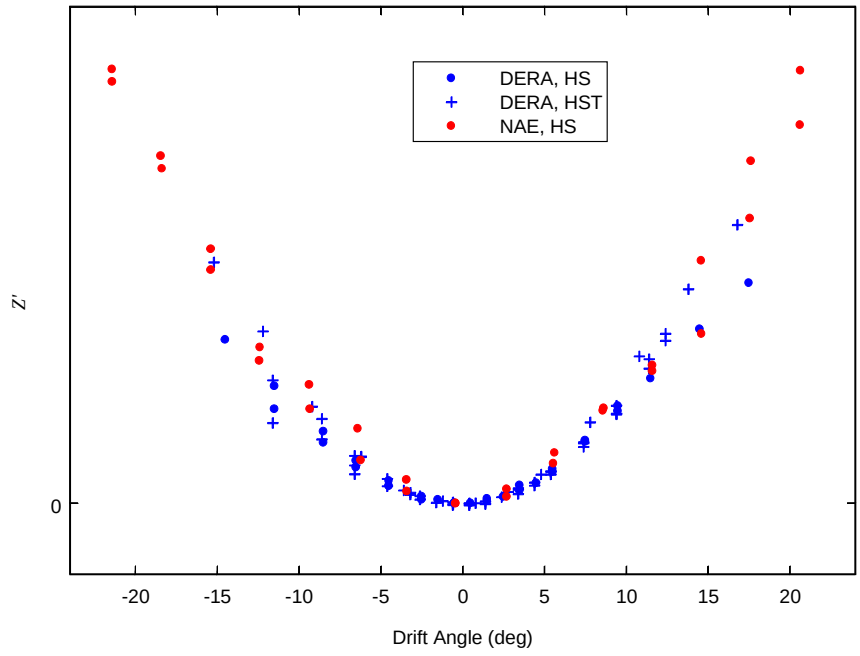


(a)

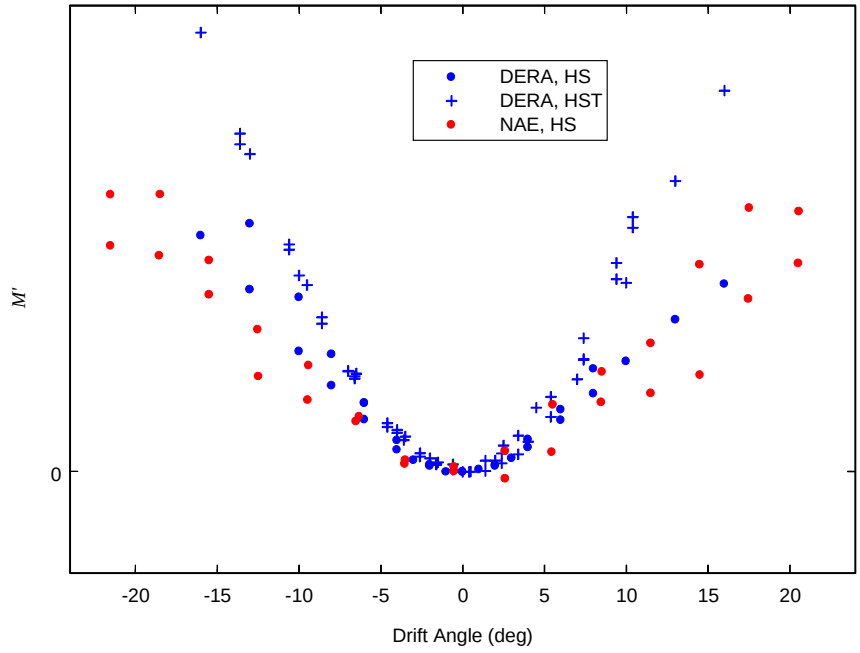


(b)

**Figure 3.** Standard Model combined data from DERA and NAE: (a) normal force and (b) pitching moment; data offsets removed.

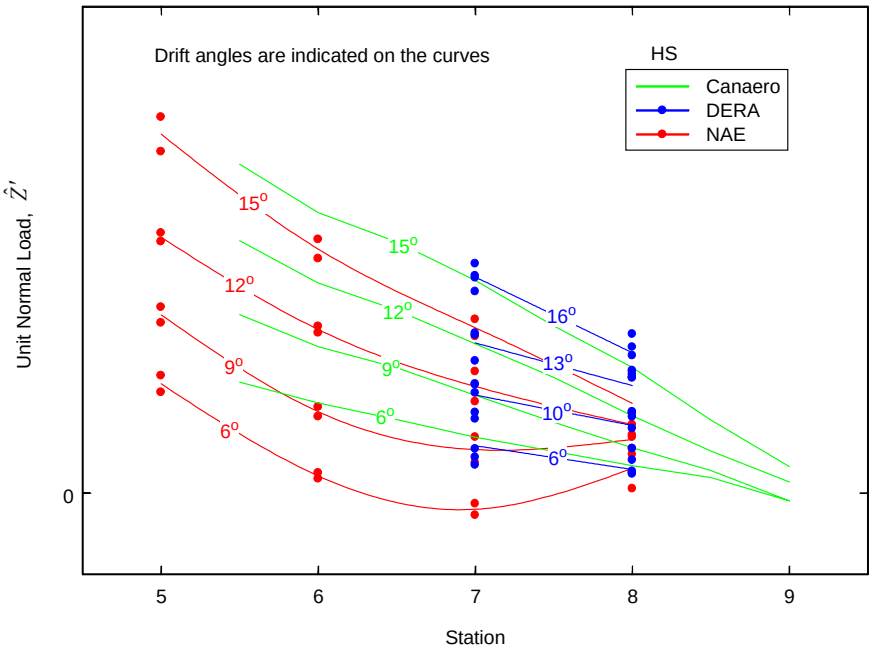


**Figure 4.** Comparison of load distributions for Standard Model HS configuration in drift.

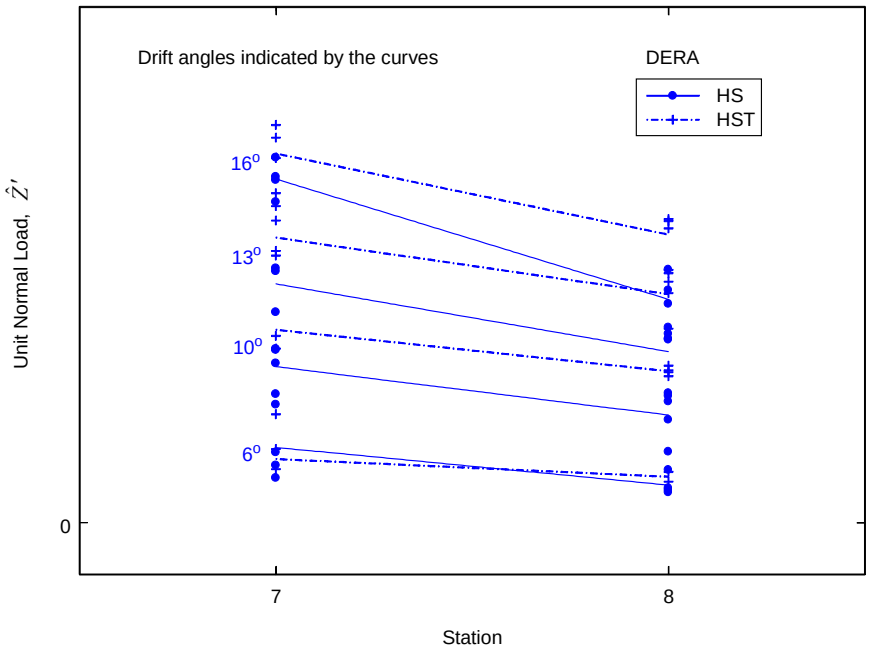


**Figure 5.** Comparison of load distributions from the DERA HS and HST experiments.

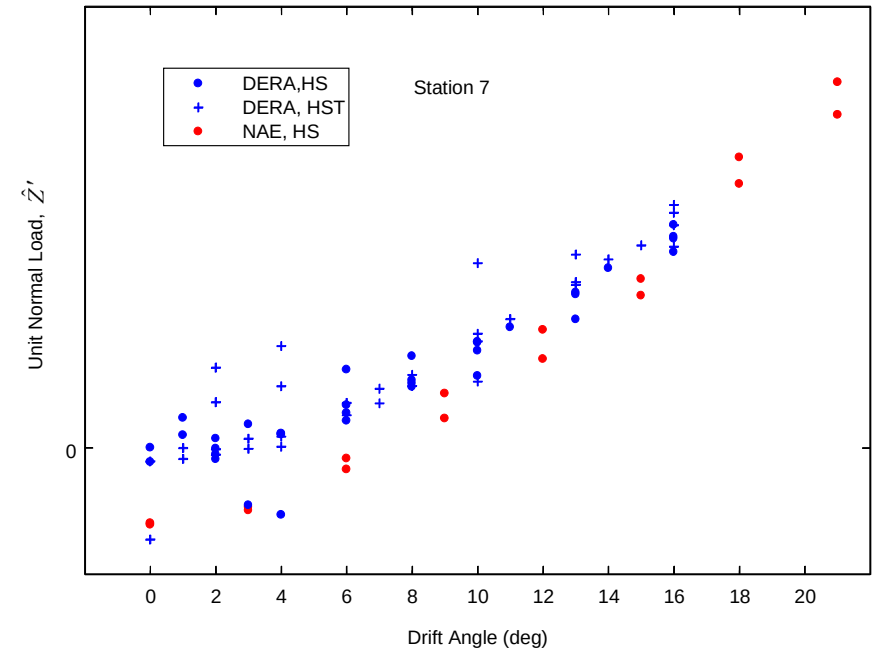


(a)

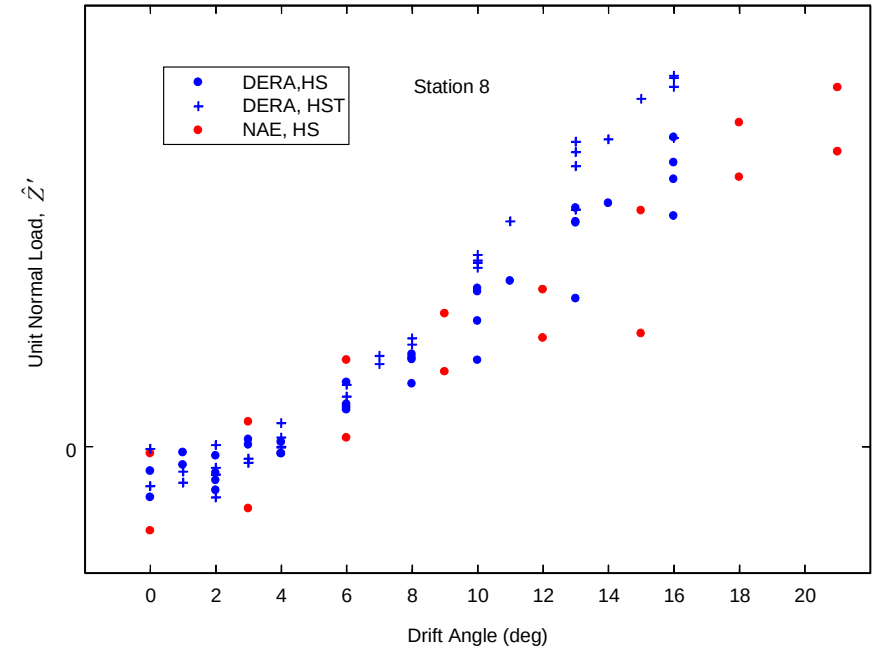


(b)

**Figure 6.** Standard Model HS and HST unit normal load at (a) station 7 and (b) station 8.

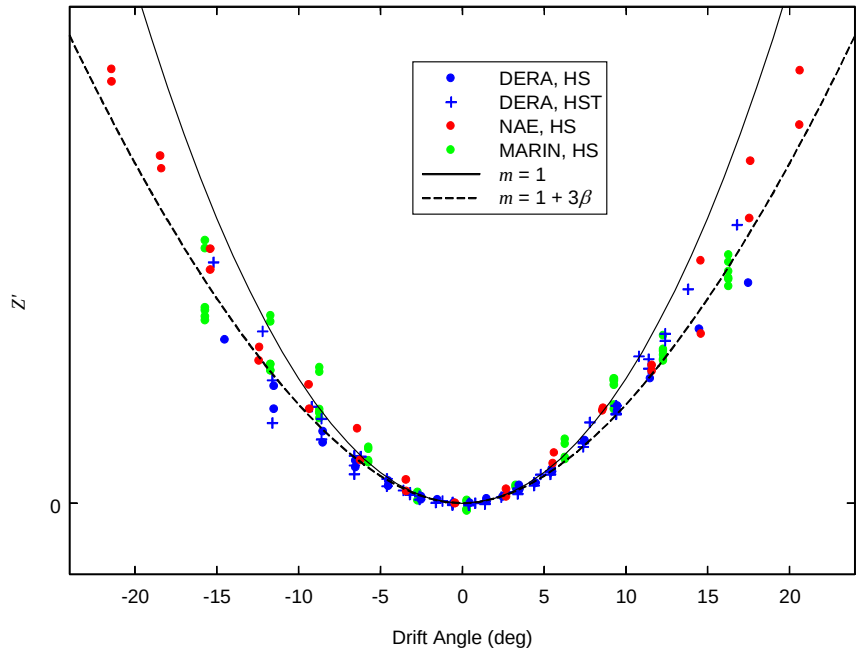


(a)

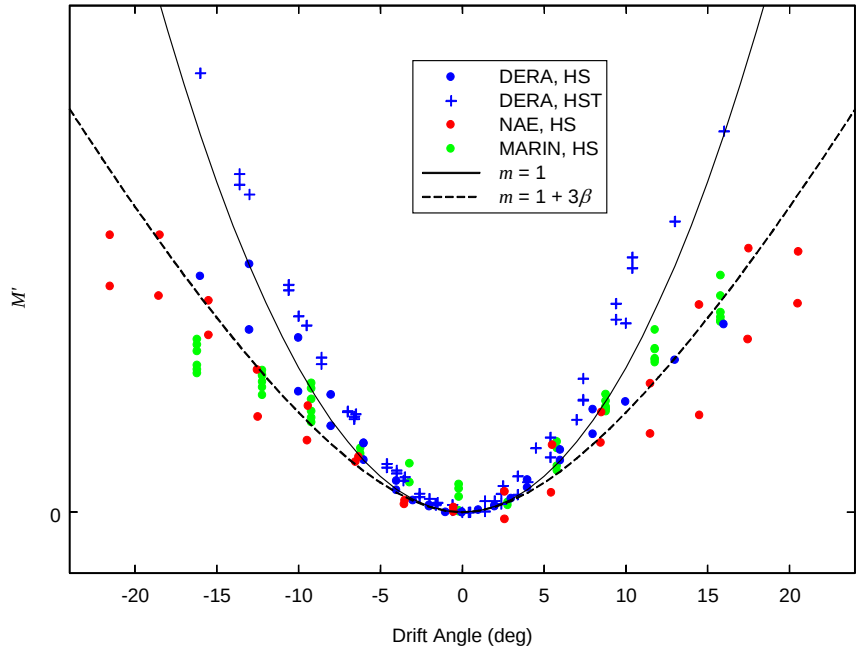


(b)

**Figure 7.** Standard Model data and predictions: (a) normal force and (b) pitching moment; data offsets removed.

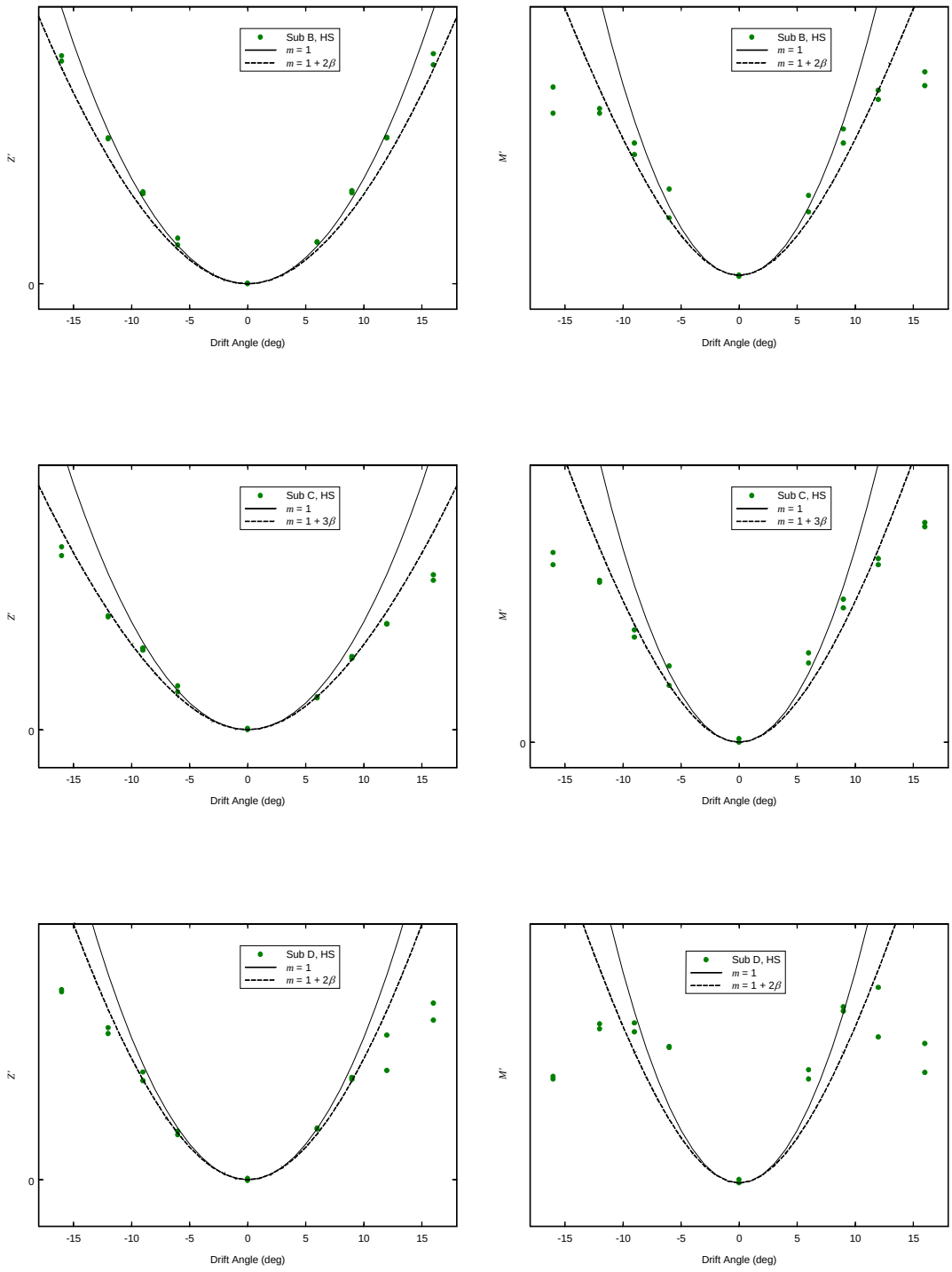


**Figure 8.** Out-of-plane load data (offsets removed) and predictions: Submarines B (top), C (middle), and D (bottom). (continued)

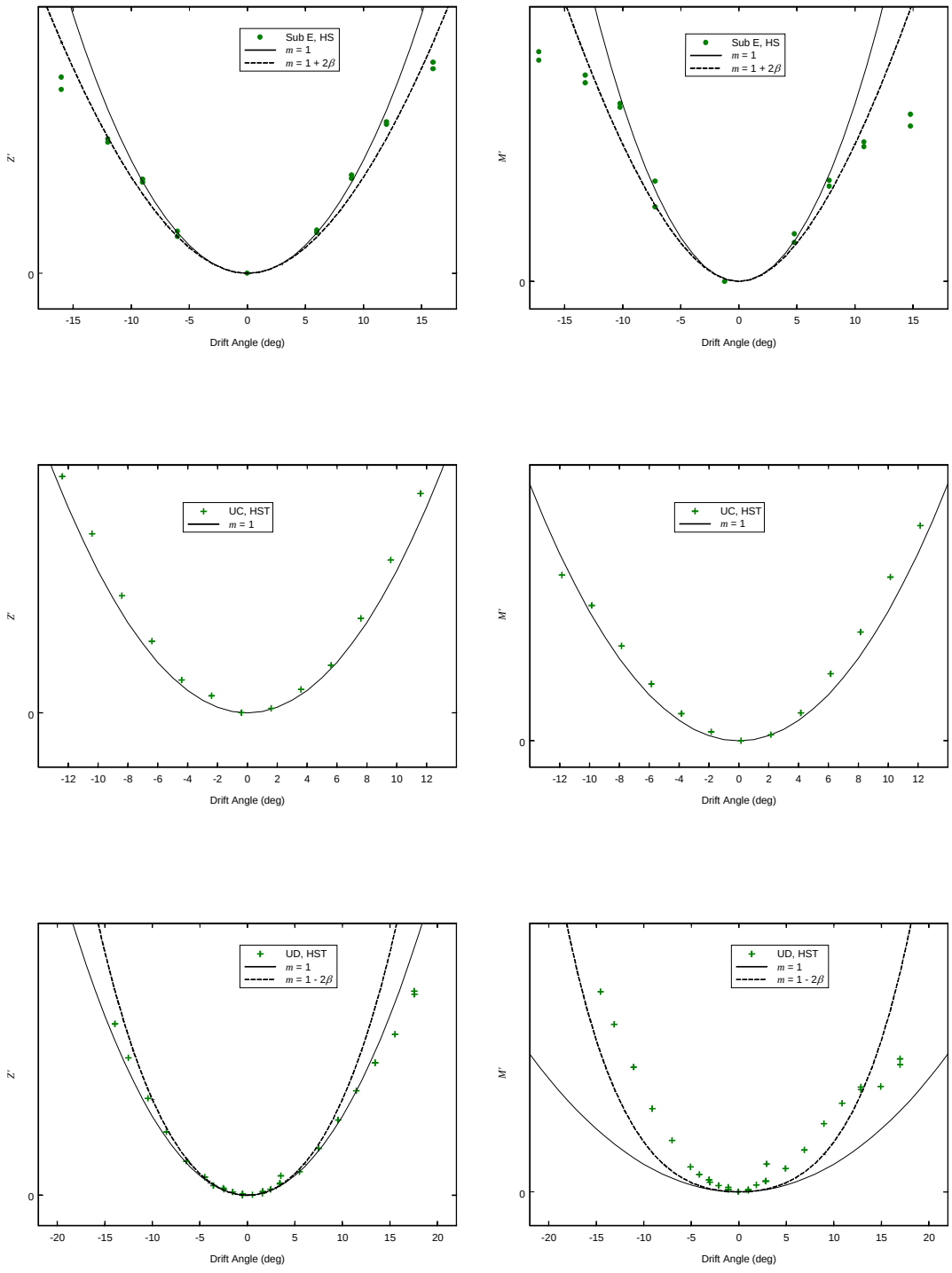


**Figure 8. (cont.)** Out-of-plane load data (offsets removed) and predictions: Submarines E (top), UC (middle), and UD (bottom). (continued)

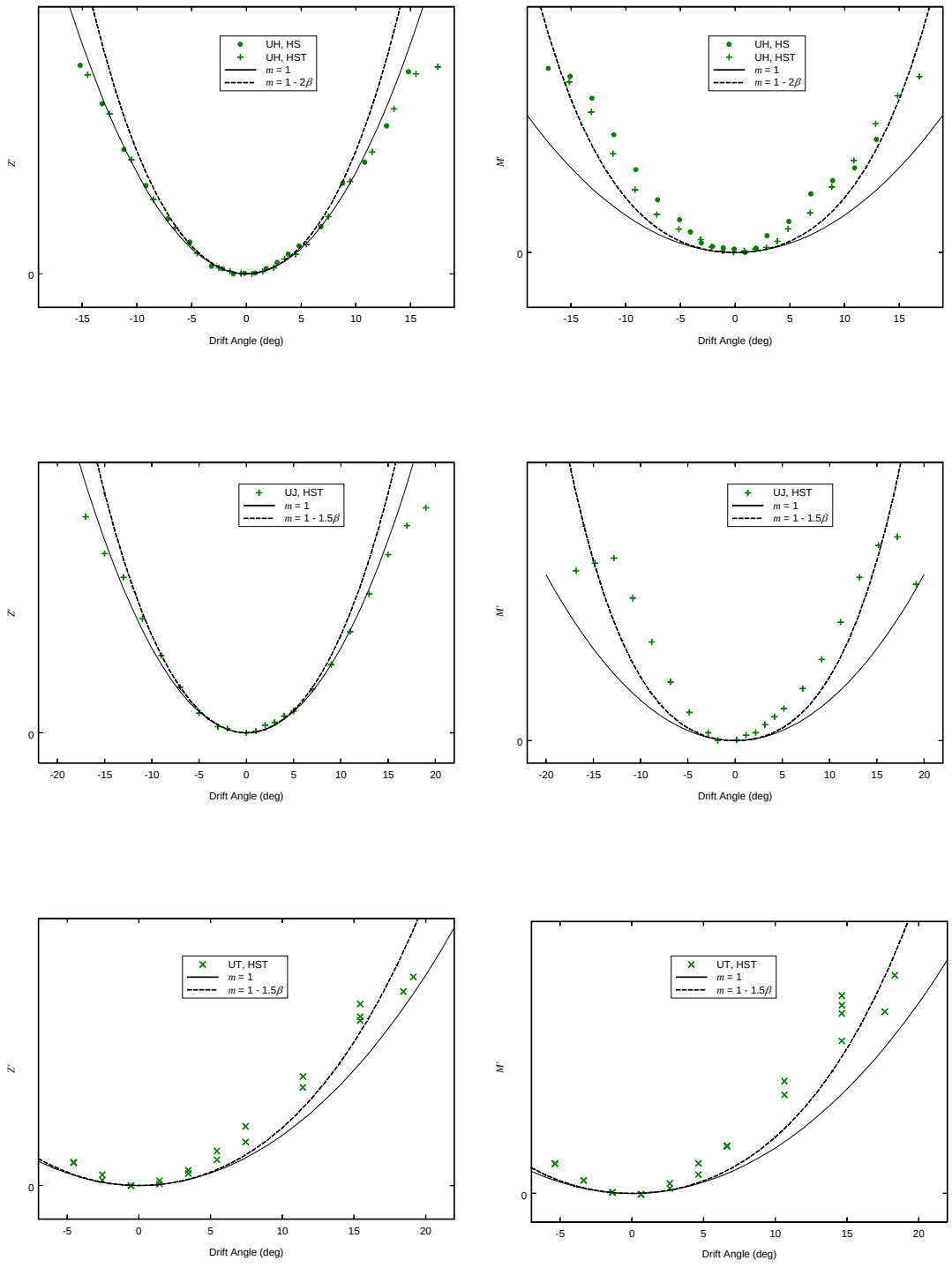


**Figure 8. (cont.)** Out-of-plane load data (offsets removed) and predictions: Submarines UH (top), UJ (middle), and UT (bottom).

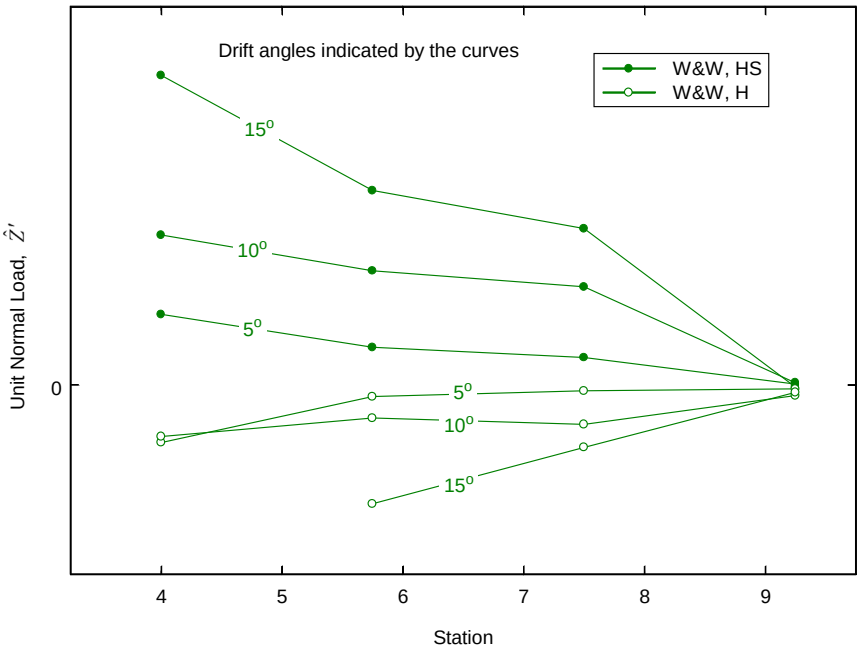


**Figure 9.** Load distributions for the Ward and Wilson model H and HS configurations; from figures 17 and 18 of reference [11].

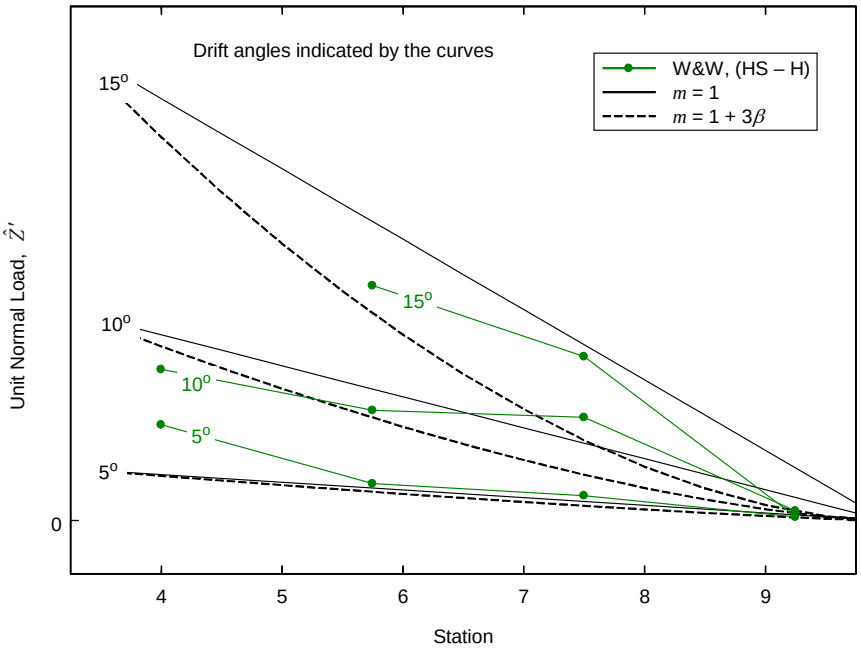


**Figure 10.** HS – H load distributions for the Ward and Wilson model compared with linear and nonlinear predictions.

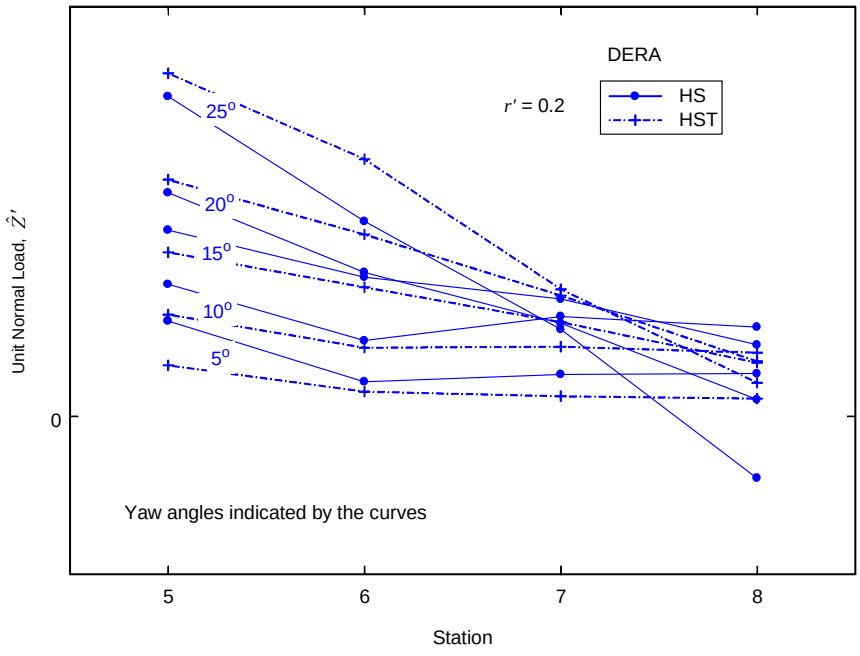


(a)

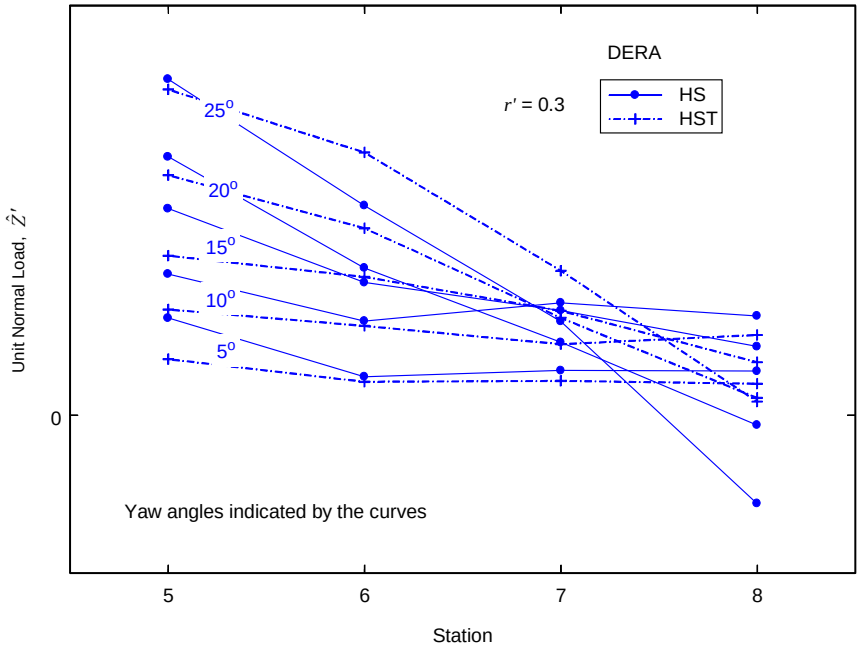


(b)

**Figure 11.** Comparison of load distributions for Standard Model HS and HST configurations on the rotating arm: (a) $r' = 0.2$ and (b) $r' = 0.3$. (continued)

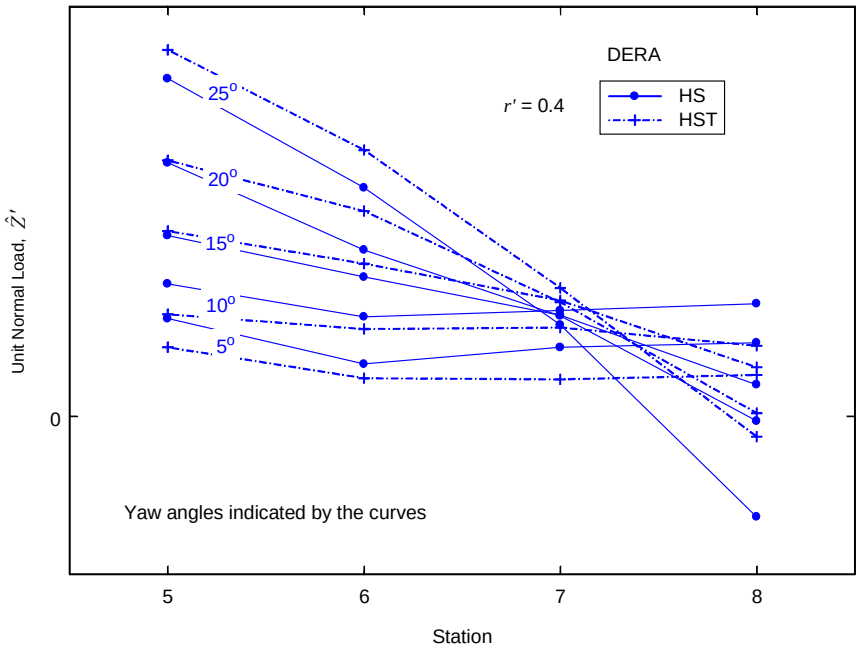


(c)

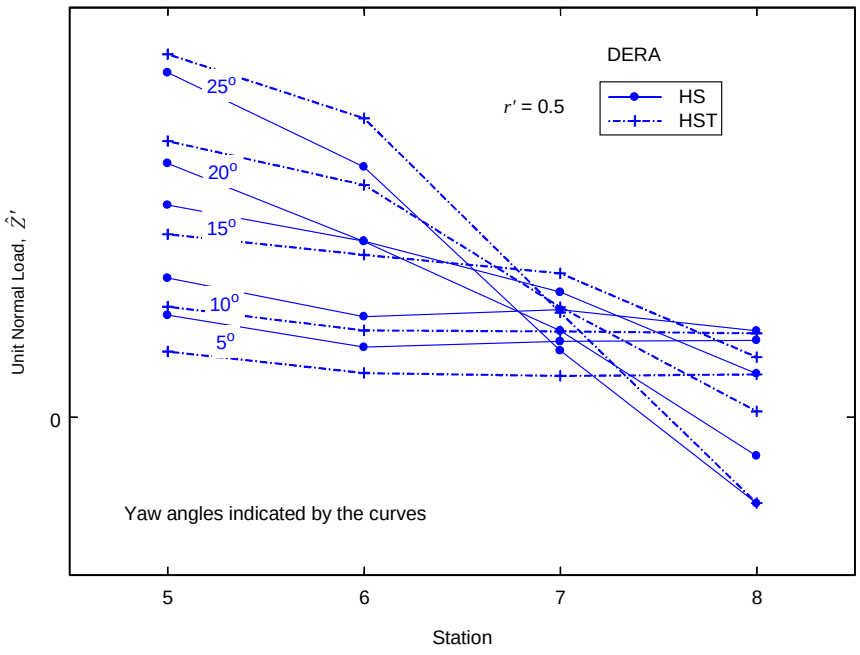


(d)

**Figure 11. (cont.)** Comparison of load distributions for Standard Model HS and HST configurations on the rotating arm: (c) $r' = 0.4$ and (d) $r' = 0.5$.

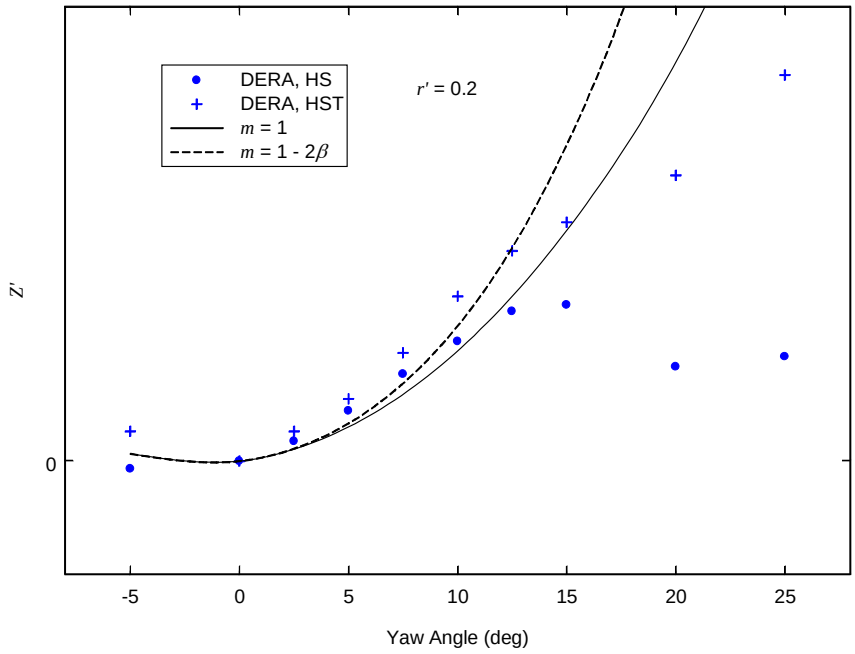


(a)

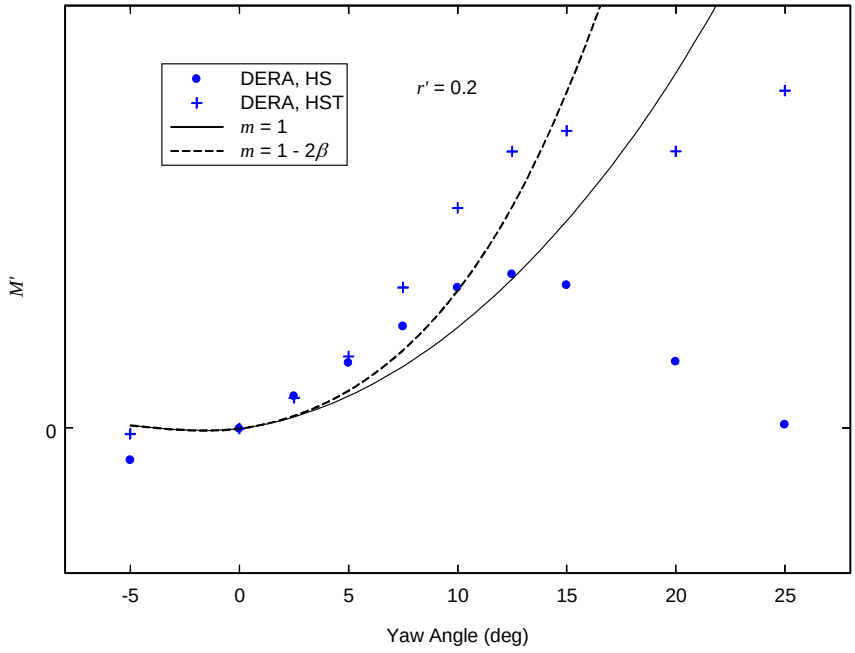


(b)

**Figure 12.** Standard Model rotating arm data and predictions, $r' = 0.2$: (a) normal force and (b) pitching moment; zero yaw data offsets removed. (continued)

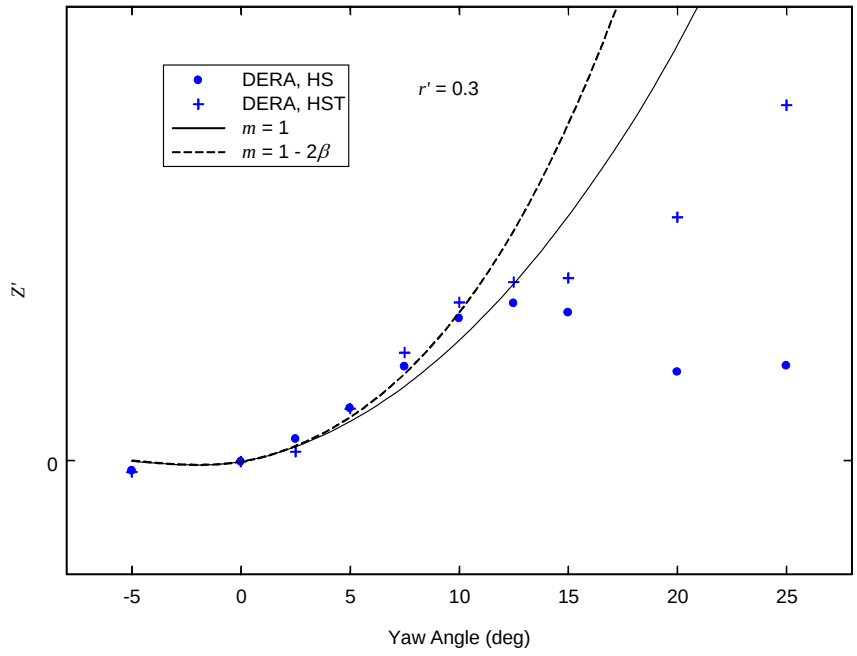


(c)

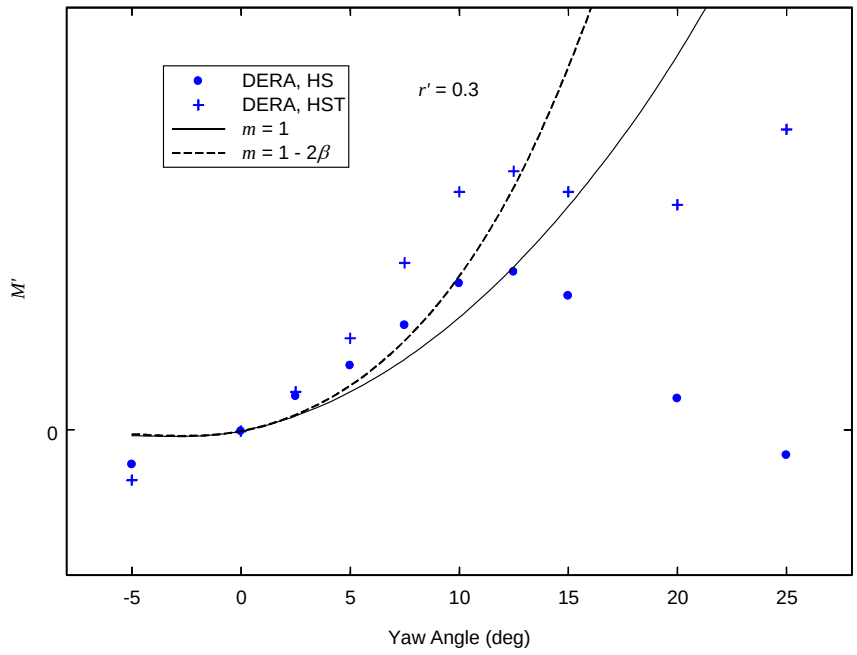


(d)

**Figure 12. (cont.)** Standard Model rotating arm data and predictions, $r' = 0.3$: (c) normal force and (d) pitching moment; zero yaw data offsets removed. (continued)

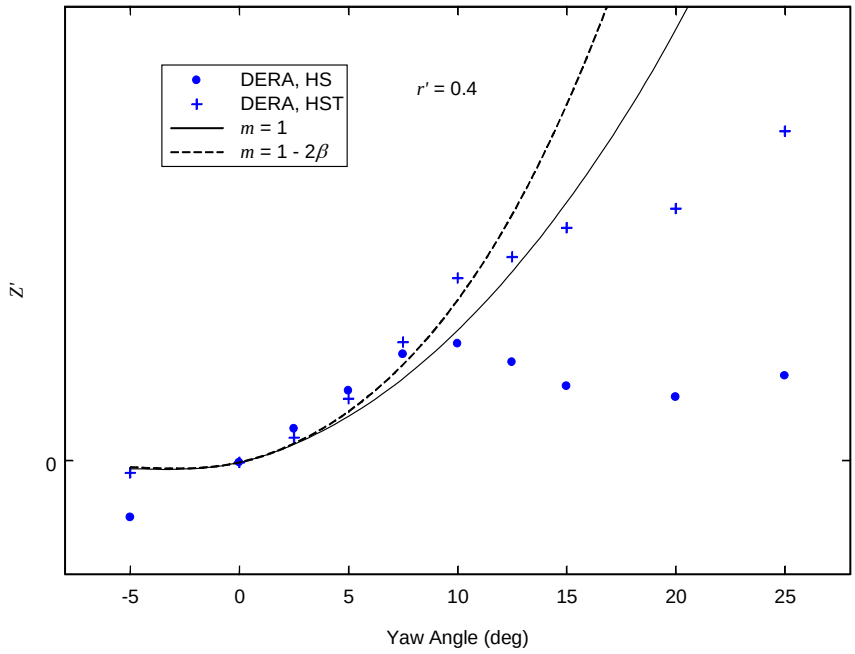


(e)

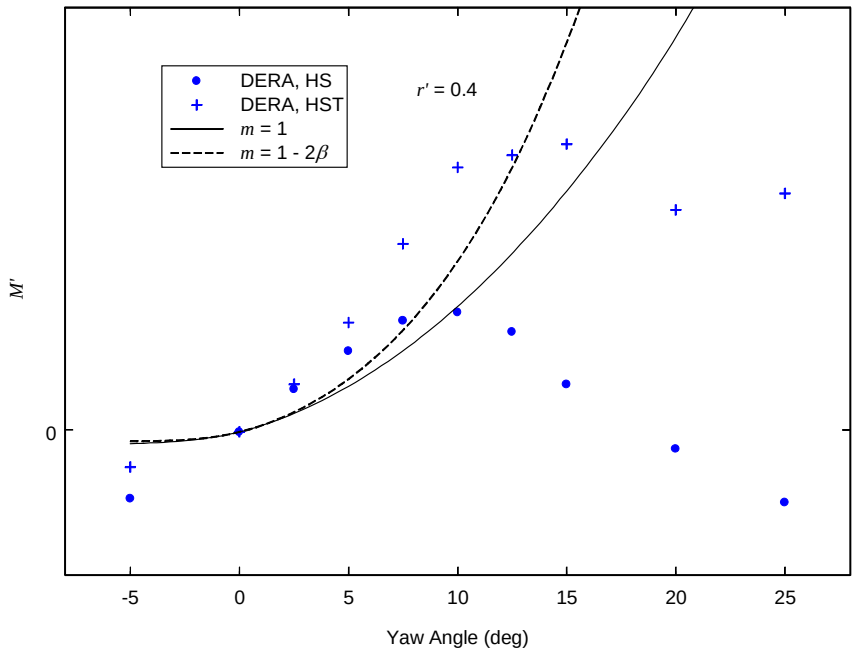


(f)

**Figure 12. (cont.)** Standard Model rotating arm data and predictions, $r' = 0.4$: (e) normal force and (f) pitching moment; zero yaw data offsets removed. (continued)

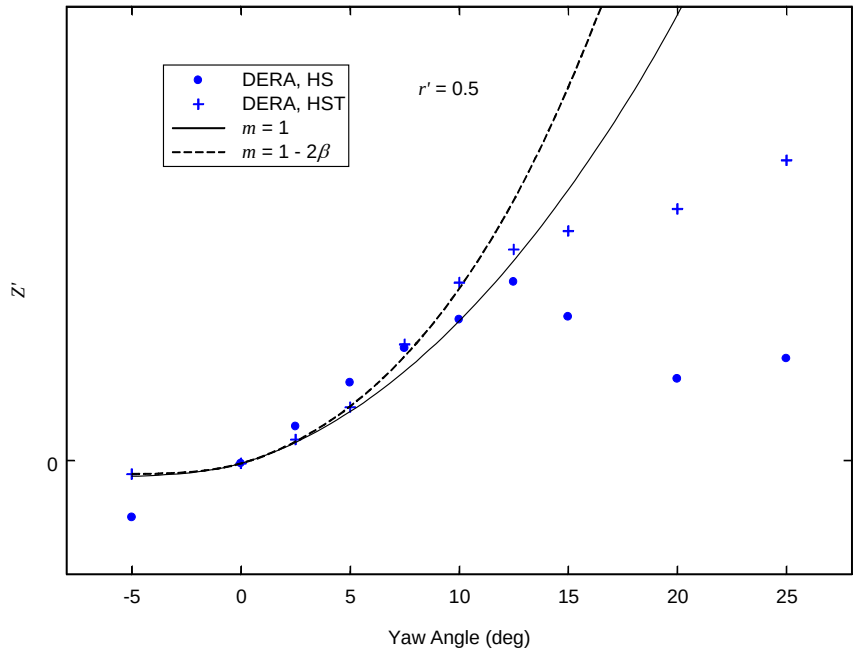


(g)

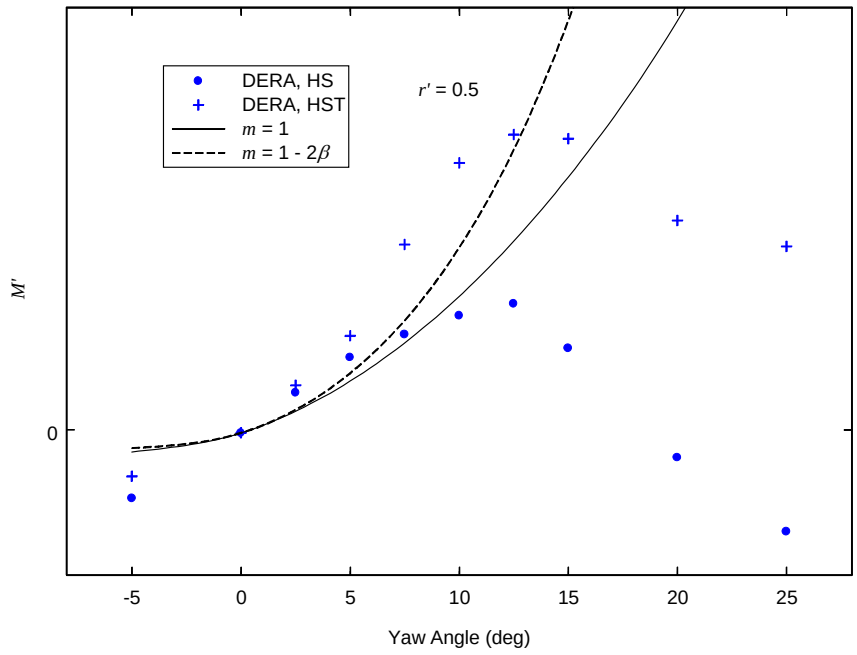


(h)

**Figure 12. (cont.)** Standard Model rotating arm data and predictions, $r' = 0.5$: (g) normal force and (h) pitching moment; zero yaw data offsets removed.

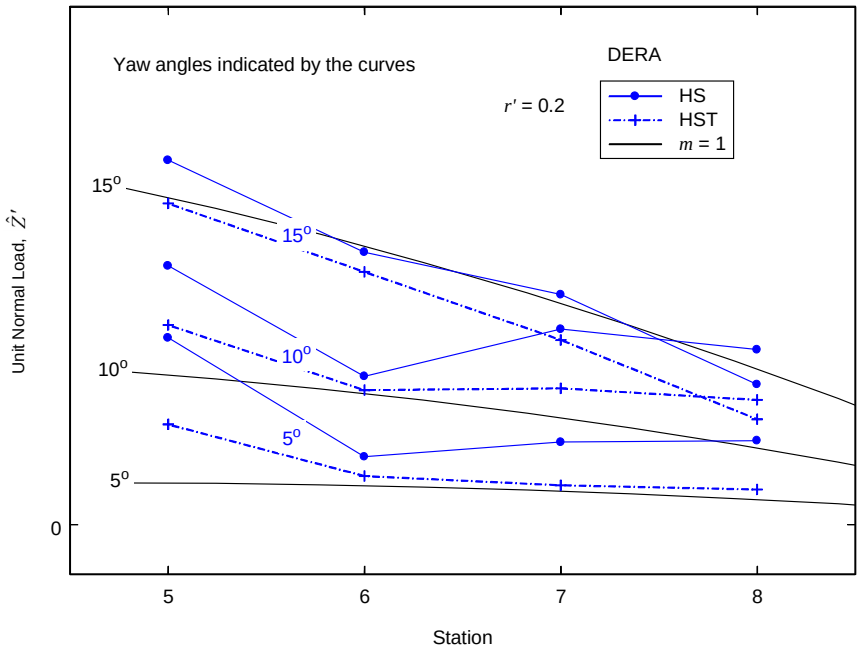


(a)

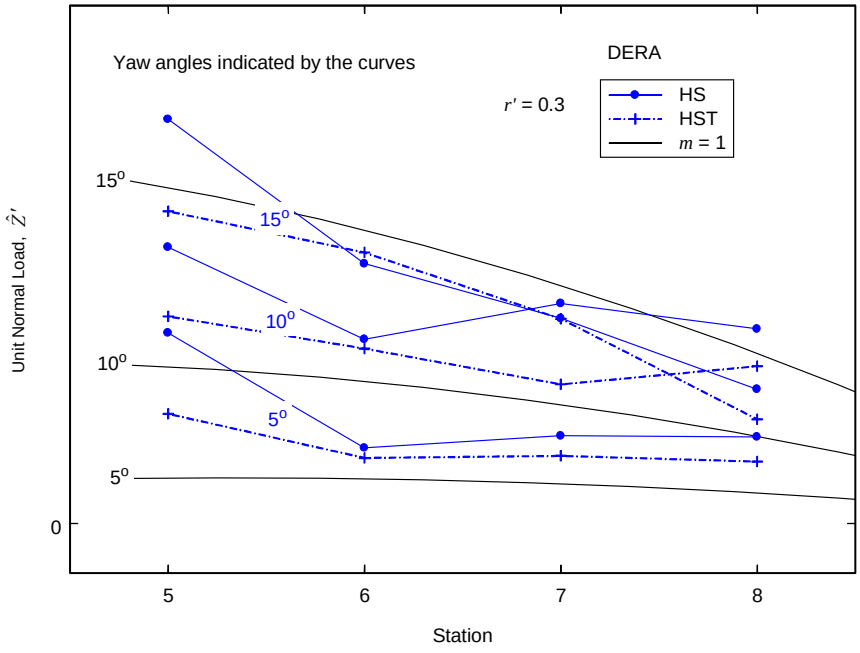


(b)

**Figure 13.** Comparison of Standard Model rotating arm load distributions and predictions: (a) $r' = 0.2$ and (b) $r' = 0.3$. (continued)

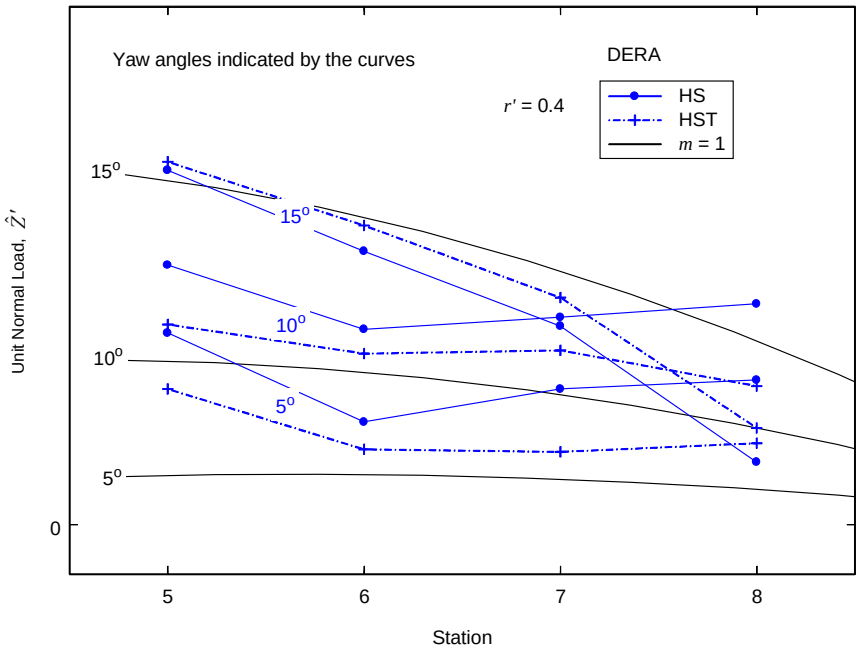


(c)

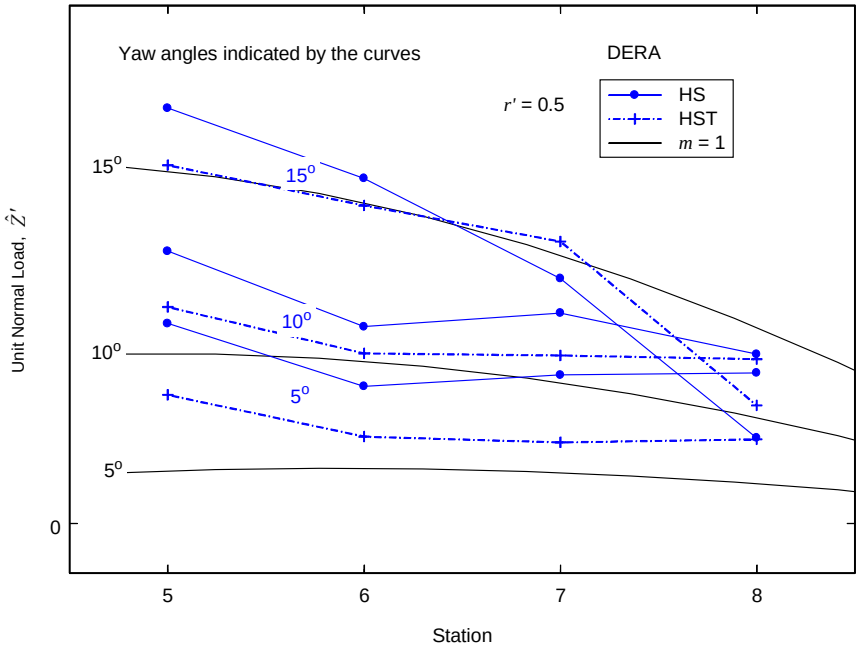


(d)

**Figure 13. (cont.)** Comparison of Standard Model rotating arm load distributions and predictions: (c) $r' = 0.4$ and (d) $r' = 0.5$.

This page intentionally left blank.

# Nomenclature

## Symbols

| | |
|---|---|
| $b_e$ | effective span of the sail |
| $f(x)$ | a distribution function |
| $L$ | hull length |
| $m$ | nonlinearity parameter in the aft loading distribution |
| $M$ | pitching moment |
| $r$ | yaw rate |
| $U$ | total velocity |
| $v$ | crossflow velocity; $v(x)$ – local value |
| $x$ | axial coordinate |
| $x_1$, $x_2$ | axial parameters in the aft loading distribution |
| $x_{AP}$ | Aft Perpendicular in axial coordinates |
| $x_{TE}$ | sail trailing edge in axial coordinates |
| $Y_{sail}$ | sail lift (sideforce) |
| $Z$ | normal force |
| $\widehat{Z}$ | normal force per unit length; $\widehat{Z}(x)$ – local value |
| $\beta$ | drift angle |
| $\beta_c$ | drift parameter in the aft loading distribution |
| $\Gamma$ | circulation, in general |
| $\Gamma_{sail}$ | sail circulation |
| $\rho$ | fluid density |

See figure 1(a) for the coordinate system convention.

Nondimensionalization is done in the standard way [4], as in the following examples:

$$x' = \frac{x}{L}, \quad v' = \frac{v}{U}, \quad r' = r\frac{L}{U}, \quad Z' = \frac{Z}{\frac{1}{2}\rho L^2 U^2}, \quad M' = \frac{M}{\frac{1}{2}\rho L^3 U^2}, \quad \text{etc.}$$

## Acronyms

| | |
|---|---|
| AP | Aft Perpendicular |
| DERA | Defence Evaluation and Research Agency |
| `DSSP20` | DRDC Submarine Simulation Program, version 2.0 |
| `DSSP21` | DRDC Submarine Simulation Program, version 2.1 |
| FP | Forward Perpendicular |
| HS | Hull and Sail configuration |
| HST | Hull, Sail, and Tail configuration |
| MARIN | Maritime Institute Netherlands |
| MDTF | Marine Dynamic Test Facility |
| NAE | National Aeronautical Establishment |
| STR | Static Test Rig |
| TE | Trailing Edge |
| UUV | Unmanned Underwater Vehicle |

## DOCUMENT CONTROL DATA

| 1. ORIGINATOR | 2. SECURITY CLASSIFICATION | |
|---|---|---|
| Defence R&D Canada – Atlantic | Unclassified | |
| **3. TITLE** | | |
| A Review of Submarine Out-of-Plane Normal Force and Pitching Moment | | |
| **4. AUTHORS** | | |
| M. Mackay | | |
| **5. DATE OF PUBLICATION** | **6a. NO. OF PAGES** | **6b. NO. OF REFS** |
| August 2004 | 33 | 11 |
| **7. DESCRIPTIVE NOTES** | | |
| DRDC Atlantic Technical Memorandum | | |
| **8. SPONSORING ACTIVITY** | | |
| | | |
| **9a. PROJECT OR GRANT NO.** | **9b. CONTRACT NO.** | |
| 11GL12, 11CL | | |
| **10a. ORIGINATOR'S DOCUMENT NUMBER** | **10b. OTHER DOCUMENT NOS.** | |
| DRDC Atlantic TM 2004–135 | | |
| **11. DOCUMENT AVAILABILITY** | | |
| Unlimited | | |
| **12. DOCUMENT ANNOUNCEMENT (if different from 11)** | | |
| | | |

**13. ABSTRACT**

This memorandum summarizes the comparison of a simple out-of-plane load estimation method with model test data for a number of submarine designs. Out-of-plane loads can be reasonably estimated from sail lift by assuming that the bound afterbody circulation falls roughly linearly to zero at the tail. Tail appendages have very little effect on these loads.

**14. KEYWORDS**

Out-of-Plane
Normal Force
Pitching Moment
Submarine

This page intentionally left blank.

This page intentionally left blank.

**Defence R&D Canada**

**Canada's leader in defence and national security R&D**

**R & D pour la défense Canada**

**Chef de file au Canada en R & D pour la défense et la sécurité nationale**


**www.drdc-rddc.gc.ca**